Aalborg Universitet

AALBORG UNIVERSITY

DENMARK

Active Damping of *LLCL*-filter Resonance Based on *LC*-Trap Voltage and Capacitor Current Feedback

Min Huang, Xiongfei Wang, Poh Chiang Loh, Frede Blaabjerg
Department of Energy Technology
Aalborg University
Aalborg, Denmark
hmi@et.aau.dk, xwa@et.aau.dk, pcl@et.aau.dk, fbl@et.aau.dk

Abstract—The *LLCL*-filter is emerging into grid-connected converters due to a smaller size compared to the conventional the *LCL*-filter. Similar to *LCL*-filter, the high order resonance introduces potential instability to the overall system which should be properly damped either passively or actively. In this paper, different feedback coefficients like the proportional, derivative, integral, high pass and low pass feedback coefficients of the filter capacitor current and the *LC*-trap circuit voltage are investigated for damping the filter resonance. Active damping methods are analyzed by using the concept of the equivalent impedance with and without the delay effect of an *LLCL*-filter based grid-connected inverter. Their corresponding equivalent circuits for the purpose of resonance damping are given to identify whether the feedback coefficient should be negative or positive for the different state-feedback methods. Then the stability of the different methods and the design of the feedback coefficient are analyzed and compared using root loci. Finally, experimental results are presented to validate the theoretical analysis.

Keywords—Active damping; LLCL-filter; grid-connected converter; impedance-based design; grid-side current control; delay; different feedback coefficients.

I. INTRODUCTION

Nowadays, distributed generation (DG) systems using clean renewable energy such as solar energy, wind energy, etc., are becoming popular in the industry [1], [2]. Regardless of the type of renewable power source, the grid-connected voltage source inverter is a crucial component that converts the energy generated by the source to the grid. Normally, a low-pass power filter is inserted between the voltage source inverter (VSI) and the grid to attenuate the undesirable harmonics caused by pulse width modulation (PWM) harmonics to a desirable limit on the grid. Typically, an *L*-filter or an *LCL*-filter is adopted to attenuate switching harmonics. Compared with *L*-filter, the *LCL*-filter is competitive for its higher attenuating ability, which allows the use of smaller inductors to meet the harmonic limits [3], [4]. Recently, a new high order filter called the *LLCL*-filter was proposed, which has a better reduction of switching harmonics with less weight and volume compared to the *LCL*-filter [5]-[8].

Similar to the *LCL*-filter, the *LLCL*-filter has also resonance problems. To suppress the possible resonance of an *LCL*-filter or *LLCL*-filter, active damping [9]-[14] or passive damping [15]-[18] methods may be adopted. A direct way to damp the resonance is to insert real resistors in the filter circuit and also

called passive damping. However additional resistors will reduce the overall system efficiency. The active damping that using control algorithm instead of the resistor has been widely explored without any additional power loss [10], they can be more effective and flexible. Among the various active damping solutions, the multi-loop active damping methods which introduces extra feedback to provide damping effect is effectively used. Normally, for the *LCL*-filter, the proportional feedback of the capacitor current is frequently used, which is equivalent to the resistor in parallel with the capacitor when the delay effect is not considered [10], [11]. Similarly, for the *LLCL*-filter, different filter variables can be measured to form a virtual resistance to damp the filter resonances [19].

However, in digital-controlled systems, sampling and transport delays caused by controller and the PWM modulation will affect the system stability and should be taken into account [20]. Due to the influence of the delay, [20] comes to the conclusion that only single grid current feedback is required at high filter resonant frequencies and in contrast only single converter side current feedback is required at low filter resonant frequencies for stability. But active damping is also required when the resonant frequency varies and grid impedance changes. Ref. [10] showed the equivalent virtual impedances of the proportional feedback of the capacitor current feedback are different considering the delay effect and it proposed a method to reduce the effect of the delay. However, the proportional feedback is not the only way to damp the resonance for the capacitor current feedback and other feedback coefficients are also effective. But there are no studies comparing these multi-loop control active damping methods and as well explaining which feedback coefficient should be used.

This paper mainly focuses on the active damping based on the *LLCL*-filter trap circuit. The *LC* trap circuit voltage and capacitor current feedback with five different general coefficients k, ks, k/s, $ks/(s+\tau)$ (high-pass), $k/(s+\tau)$ (low-pass) are analyzed and compared, when the grid-side current is controlled. It shows also how to define the k and τ, when different active damping methods are used to keep the system stable. In section II shows the modeling of the grid-connected inverter with the *LLCL*-filter. Section III, the equivalent impedances of the difference state-feedback methods are deduced with and without taking into account delays. In Section IV the stability and robustness of different cases are
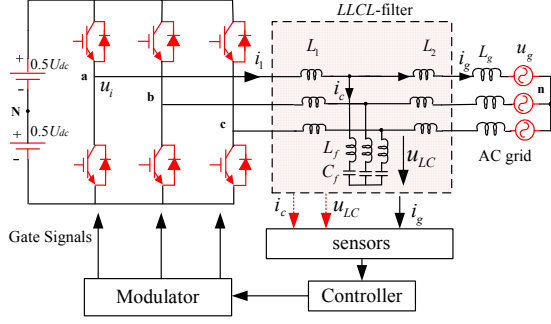
Fig. 1. General structure of three-phase grid-connected inverter with *LLCL*-filter.

analyzed by root loci in the discrete domain. Last, experimental results are provided to validate the theoretical analysis.

II. MODELING THE GRID-CONNECTED INVERTER WITH THE *LLCL*-FILTER

A. System Description

Fig. 1 shows the general structure of a three-phase grid-connected inverter with *LLCL*-filter. The DC-link voltage is assumed to be constant. L_1 is the inverter-side inductor, C_f is the filter capacitor, L_f is the resonant inductor and L_2 is the grid-side inductor. The voltage and current of the inverter output phase are represented as u_i and i_1, and the grid voltage and current are represented as u_g and i_g. The voltage of the trap circuit L_f-C_f is u_{LC}, i_c is the capacitor current, and L_g is the grid impedance. Table I shows the parameters of the system.

As shown in Fig. 1, the grid-side current is controlled. The feedback signal i_c and u_{LC} can be used to damp the resonance of the *LLCL*-filter. The open loop transfer function from i_g to u_i is expressed in (1). The resonance frequency of the *LLCL*-filter ω_r ($\omega_o = 2\pi f_o$) is derived in (2).

$$G_{u_i \rightarrow i_g}(s) = \frac{L_f C_f s^2 + 1}{C_f [L_1 L_2 + (L_1 + L_2) L_f] s (s^2 + \omega_r^2)} \quad (1)$$

$$\omega_r = \frac{1}{\sqrt{\left(\dfrac{L_1 L_2}{L_1 + L_2} + L_f\right) C_f}} \quad (2)$$

The Proportional-Resonant with the Harmonic-Compensation (PR+HC) controller can be used in the current controller [21]. In the s-domain, the current controller is expressed as:

$$G_c(s) = K_p + \sum_{h=1,5,7} \frac{K_{ih} s}{s^2 + (\omega_0 h)^2} \quad (3)$$

where $\omega_o = 2\pi f_o$ is the fundamental angular frequency, K_p is the proportional gain, and K_{ih} is the integral gain of the individual resonant frequency h.

B. Active Damping Based on LC-trap

According to [14] and [22] different feedback variables are feasible for damping the resonant problems. Capacitive

TABLE I
Parameters of System

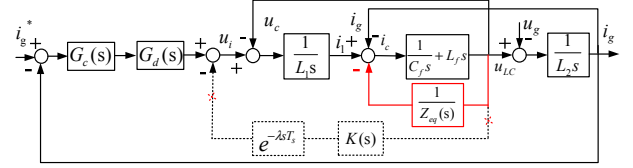| DC link voltage U_{dc}	650 V	Sampling frequency f_s	10 kHz
Grid phase voltage U_g	220 V	Resonant frequency f_r	2.45 kHz
Inductor L_1	1.8 mH	Grid-side inductor L_2	2 mH
Capacitor C_f	4 μF	Resonant inductor L_f	64 μH
Switching frequency f_{sw}	10 kHz	Sampling period T_s	100 μs

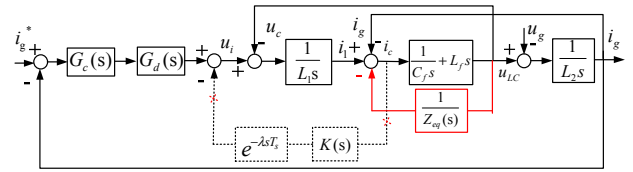Fig. 2. Equivalent block diagram of grid current control with L_f-C_f trap voltage feedback.

Fig. 3. Equivalent block diagram of grid current control with capacitor current feedback.

voltage is relatively easy to measure and can also be used for synchronization, so the capacitor voltage is usually used as a feedback variable. Fig. 2 shows the structure of an active damping method based on the L_f-C_f trap voltage for grid-connected VSI with *LLCL*-filter. $K(s)$ is the feedback coefficient. Delay part is modelled as $G_d(s) = e^{-\lambda s T_s}$ where T_s is the sampling period and λ is the delay coefficient. PWM inverter transfer function is expressed as $K_{PWM} = V_{in}/V_{tri}$, where V_{in} is the input voltage, and V_{tri} is the amplitude of the triangular carrier. If the voltage V_{tri} is the same as V_{in}, K_{PWM} can be regarded as 1.

When the feedback node is moved from the output of $G_d(s)$ to the output node of $1/sL_1$, an equivalent block diagram of the equivalent virtual impedance is obtained, as shown in Fig. 2 with a solid line. The L_f-C_f trap voltage based active damping is equivalent to the virtual impedance $Z_{eq}(s)$ in parallel with L_f-C_f trap circuit. Computational and PWM delays are introduced into the grid current loop and the active damping feedback circuit.

Similar to L_f-C_f trap voltage based active damping method the capacitor current can also be sensed to damp the resonance. The structure of the active damping method based on the L_f-C_f trap voltage for grid-connected VSI with *LLCL*-filter is shown in Fig. 3. When the feedback node is moved from the output of $G_d(s)$ to the current output node of $1/sL_1$ and the initial feedback variable is moved from i_c to u_{LC}, an equivalent block diagram of the equivalent virtual impedance is obtained.

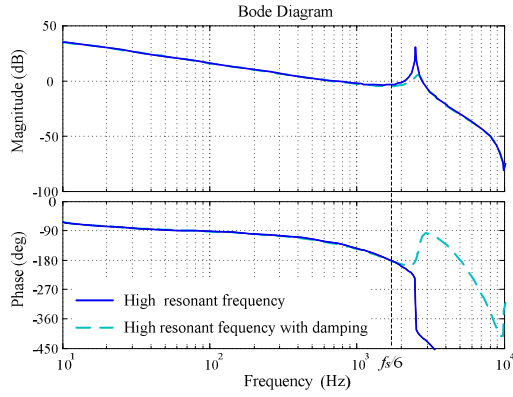The open loop transfer functions from i_c to u_i and u_{LC} to u_i are expressed in (4) and (5), respectively.

Fig. 4. Bode plot of the of transfer functions i_g (s) / u_i (s) with and without damping in high resonant frequency.

$$G_{u_i \to i_c}(s) = \frac{L_2 s^2}{[L_1 L_2 + (L_1 + L_2)L_f]s(s^2 + \omega_r^2)} \quad (4)$$

$$G_{u_i \to u_{LC}}(s) = \frac{L_2 s(L_f C_f s^2 + 1)}{C_f[L_1 L_2 + (L_1 + L_2)L_f]s(s^2 + \omega_r^2)} \quad (5)$$

Fig. 4 shows the Bode plot of the of transfer functions i_g (s) / u_i (s) when λ is 1.5. It can be seen from Fig. 4, that the *LLCL*-filter resonance has no influence on system stability since the phase is already well below -180º at f_s/6 due to the sampling and transport delays [10]. Here, f_s is the sampling frequency and f_s/6 is called the critical frequency. But the resonance frequency will be changed when grid impedance varies, so active damping is still necessary in order to improve the robustness. As shown in Fig. 4, when the proportional capacitor-current-feedback active damping is used if the resonant frequency is larger than one-sixth of the sampling frequency (f_s /6) the phase will cross -180 º twice, because a non-minimum phase behavior of the outer grid current control loop is introduced by the negative virtual impedance of the active damping. A stability analysis should be carried out by means of the Nyquist stability criterion. In order to get the system stable, the magnitude margin at f_s /6 should be larger than 0 and the magnitude margin at the resonance frequency f_r should be smaller than 0 [10]. But in a weak grid, the resonance frequency will probably be decreased below f_s /6, so if the critical frequency can be increased the robustness against the grid-impedance variation can be better. Ref. [10] reduces the computational delay by shifting the capacitor current sampling instant towards the PWM reference update instant to get a wider frequency. The critical frequency is changed from f_s /6 to f_s /4 for the proportional capacitor-current-feedback active damping.

The next section will analyze the impedance-based active damping methods in more details.

III. IMPEDANCE-BASED ACTIVE DAMPING ANALYSIS

A. Virtual Impedance Model

The parameter $K(s)$ is discussed from five different coefficients: k, ks, k/s, $ks/(s+\tau)$, $k/(s+\tau)$. When k is larger than zero, it is feedback control and when k is smaller than zero, it
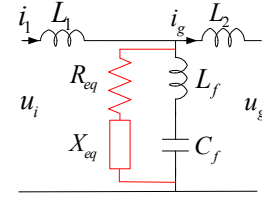

Fig. 5. Equivalent circuit considering delay.

is feedforward control. Ref. [11] analyzed the influence of different resonant frequencies for proportional capacitor current feedback. For grid current control with L_f-C_f trap voltage feedback, Z_{eq}(s) is expressed as:

$$Z_{eq}(s) = s \cdot L_1 / K(s) \cdot e^{\lambda s T_s} \quad (6)$$

For grid current control with capacitor current feedback, Z_{eq}(s) is expressed as:

$$Z_{eq}(s) = \frac{L_1(1 + s^2 L_f C_f)}{C_f K(s)} \cdot e^{\lambda s T_s} \quad (7)$$

Substituting (8) into (6) and (7), a general Z_{eq} is expressed as (9). Fig. 5 shows the general equivalent circuit considering the delay. R_{eq} is the equivalent resistance part of Z_{eq} and X_{eq} is the equivalent inductive or capacitive part of Z_{eq}.

$$e^{j\omega\lambda T_s} = \cos\omega\lambda T + j\sin\omega\lambda T \;,\; s \to j\omega \quad (8)$$

$$Z_{eq}(j\omega) = R_{eq}(\omega) + jX_{eq}(\omega) \quad (9)$$

R_{eq} and X_{eq} are frequency dependent. The actual *LLCL*-filter resonance frequency is probably changed by the imaginary part of the virtual impedance X_{eq}. The real part of the virtual impedance might be negative and it is relative to the ratio of the *LLCL* resonance frequency to the control frequency. The negative resistance brings in open-loop
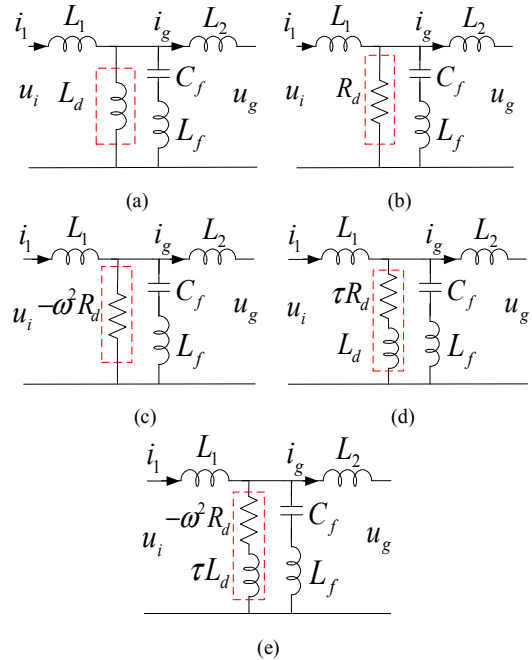

Fig. 6. Equivalent virtual impedances of the L_f- C_f voltage feedback without delay. (a) k, (b) ks, (c) k/s, (d) $ks/(s+\tau)$, (e) $k/(s+\tau)$.

TABLE II

R_{eq} and X_{eq} of Equivalent Virtual Impedances for the L_f- C_f Trap Voltage feedback

$K(s)$	k	ks	k/s	$ks/(s+\tau)$	$k/(s+\tau)$
$R_{eq}(\omega)$	$-\dfrac{L_1\omega}{k}\cdot\sin\lambda\omega T_s$	$\dfrac{L_1}{k}\cdot\cos\lambda\omega T_s$	$\dfrac{-L_1\omega^2}{k}\cdot\cos\lambda\omega T_s$	$\dfrac{L_1\tau}{k}\cdot\cos\lambda\omega T_s-\dfrac{L_1\omega}{k}\cdot\sin\lambda\omega T_s$	$-\dfrac{L_1\omega^2}{k}\cdot\cos\lambda\omega T_s-\dfrac{L_1\tau\omega}{k}\cdot\sin\lambda\omega T_s$
$X_{eq}(\omega)$	$\dfrac{L_1\omega}{k}\cdot\cos\lambda\omega T_s$	$\dfrac{L_1}{k}\cdot\sin\lambda\omega T_s$	$-\dfrac{L_1\omega^2}{k}\cdot\sin\lambda\omega T_s$	$\dfrac{L_1\tau}{k}\cdot\sin\lambda\omega T_s+\dfrac{L_1\omega}{k}\cdot\cos\lambda\omega T_s$	$-\dfrac{L_1\omega^3}{k}\cdot\sin\lambda\omega T_s+\dfrac{L_1\tau\omega}{k}\cdot\cos\lambda\omega T$
f_n	$f_s/3$	$f_s/6$	$f_s/6$	see Fig. 7(a)	see Fig. 7(b)

unstable Right Half-Plane (RHP) poles into the grid current control loop.

B. Virtual Impedance Model of the L_f-C_f Trap Voltage Based Active Damping

Table II shows the equivalent R_{eq} and X_{eq} with different feedback coefficients of L_f - C_f voltage feedback. In the continuous time domain, it is easy to deduce the physical equivalences and stability conditions for the active damping control loop. When $\lambda=0$, Fig. 6 shows the equivalent circuits of L_f - C_f voltage feedback without delay effect. R_d and L_d are shown in (10).

$$R_d=\frac{L_1}{k}, \ L_d=\frac{j\omega L_1}{k} \quad (10)$$

When the delay is considered, R_{eq} could both be negative or positive and also the resonant frequency of the $LLCL$-filter will be changed by the virtual impedance. It can be seen from Table II that the L_f-C_f trap voltage with k, k/s and $k/(s+\tau)$ feedback have negative resistance R_{eq} at low frequency, so k should be negative to get the damping effect and this method can be regarded as feedforward. The L_f-C_f trap voltage with ks and $ks/(s+\tau)$ feedback have positive resistance R_{eq} at low
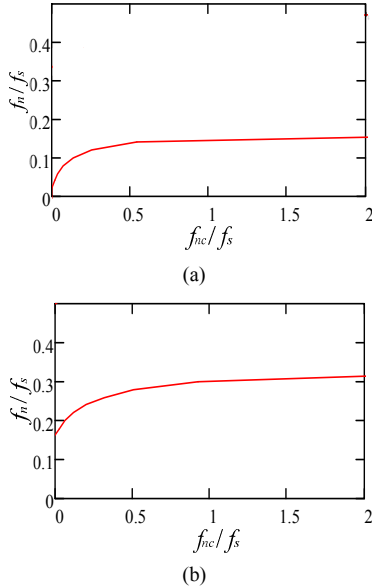
(a)

(b)

Fig. 7. Relationship between the frequency when the virtual resistance becomes negative and the cut-off frequency of the filter using the L_f- C_f voltage feedback. (a) $ks/(s+\tau)$, (b) $k/(s+\tau)$.
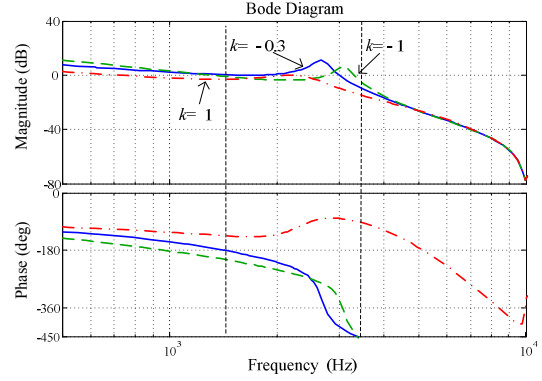

Fig. 8. Bode plot of the open-loop gain of the grid current control with the L_f-C_f trap voltage with k feedback (-1, -0.3, 1).

frequency and k should be positive in order to get the damping effect and this method can be regarded as feedback control.

Table II shows the frequency f_n at which the real part of the virtual impedance becomes negative (f_n) before Nyquist frequency. It can be seen from Table II that L_f-C_f trap voltage active damping with k feedforward has a larger critical frequency f_n. It means the actual resonance frequency is higher than one-third of the sampling frequency (f_s /3), where the virtual impedance contains a negative resistive component. The critical frequencies of L_f-C_f trap voltage active damping with $ks/(s+\tau)$ feedback and $k/(s+\tau)$ feedback are dependent on the cut-off frequency f_{nc} ($\tau=2\pi f_{nc}$). It can be seen from Fig. 7, the critical frequency is increased when f_{nc} is increasing.

Fig. 8 shows the Bode plot of the open loop gain when the L_f-C_f trap voltage with k feedback is used. When k is smaller than 0 the open-loop unstable poles have been removed and the phase at f_r is already well below $-180°$. When k is equal to -0.3, the phase margin is very small.

C. Virtual Impedance Model of the Capacitor Current Based Active Damping

Table III shows the equivalent resistance R_{eq} and reactance X_{eq}, where A, B, C are expressed as:

$$A=\frac{L_1\left(1-\omega^2 L_f C_f\right)}{C_f k}, B=\frac{L_1\left(1-\omega^2 L_f C_f\right)}{\omega C_f k}, C=\frac{L_1\omega}{C_f k}-\frac{L_1 L_f\omega^3}{k} \quad (11)$$

They are always larger than zero before switching frequency. So the effect of L_f to the active damping can be neglected before the Nyquist frequency and the L_f-C_f circuit features like a capacitor, which is similar to the LCL-filter. When $\lambda=0$, Fig. 9 shows the equivalent circuits of capacitor current feedback without any delay effect.

TABLE III
R_{eq} and X_{eq} of Equivalent Virtual Impedances of L_f- C_f Trap Current Feedback

$K(s)$	k	ks	k/s	$ks/(s+\tau)$	$k/(s+\tau)$
$R_{eq}(\omega)$	$A\cos\lambda\omega T$	$B\sin\lambda\omega T$	$-C\sin\lambda\omega T$	$A\cos\lambda\omega T + B\tau\sin\lambda\omega T$	$\tau A\cos\lambda\omega T - C\sin\lambda\omega T$
$X_{eq}(\omega)$	$A\sin\lambda\omega T$	$-B\cos\lambda\omega T$	$C\cos\lambda\omega T$	$A\sin\lambda\omega T - \tau B\cos\lambda\omega T$	$\tau A\sin\lambda\omega T + C\cos\lambda\omega T$
f_n	$f_s/6$	$f_s/3$	$f_s/3$	see Fig. 10(a)	see Fig. 10(b)

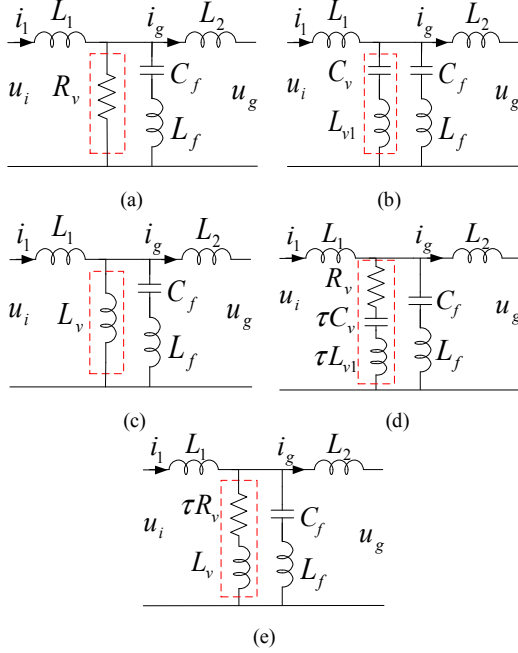Fig. 9. Equivalent virtual impedances of the capacitor current feedback without delay. (a) k, (b) ks, (c) k/s, (d) $ks/(s+\tau)$, (e) $k/(s+\tau)$.

where R_v, L_v, L_{v1} and C_v are derived as:

$$R_v = \frac{L_1\left(1-\omega^2 L_f C_f\right)}{C_f k}, \quad L_v = j\left(\frac{L_1\omega}{C_f k} - \frac{L_1 L_f \omega^3}{k}\right) \tag{12}$$

$$L_{v1} = \frac{j\omega L_1 L_f}{k}, \quad C_v = \frac{L_1}{j\omega C_f k} \tag{13}$$

The capacitor current feedback with high pass active damping is a virtual series R-C damper in parallel with the filter capacitor. When the delay effect is considered, with capacitor current k, ks, $ks/(s+\tau)$ and $k/(s+\tau)$ feedback, the equivalent impedances have positive resistance part R_{eq} at low frequency, so k should also be positive. For $k/(s+\tau)$ and $ks/(s+\tau)$ feedback, the f_n is dependent on the cut-off frequency f_{nc}, as shown in Fig. 10.

It can be seen from Fig. 10(a), the critical frequency of the capacitor current feedback with high pass active damping increases with the cut-off frequency and it is higher than the proportional capacitor current feedback [12]. The stability and robustness analysis of these methods will be shown in the next section.
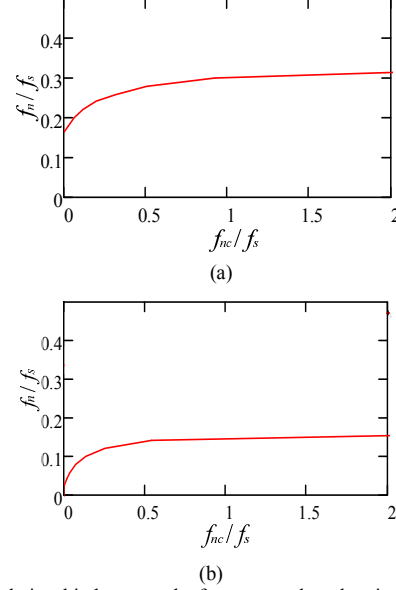

Fig. 10. Relationship between the frequency when the virtual resistance becomes negative and the cut-off frequency of the filter using the capacitor current feedback. (a) $ks/(s+\tau)$, (b) $k/(s+\tau)$.
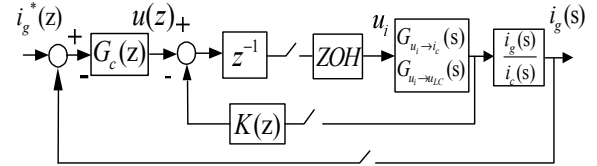

Fig. 11. Block diagram for active damping using a digital controller.

IV. ROOT-LOCUS ANALYSIS IN THE DISCRETE Z-DOMAIN

A. Modeling of Active Damping in Discrete Time

As shown in the Fig. 11, the continuous *LLCL*-filter model is discretized by a zero-order hold method with a discrete-time active damping control [23]. The feedback function $K(s)$ is discretized by the tustin method and λ is 1.5. To investigate the critical situation, the critical gain of the controller K_p can be found from the root locus analysis. (14) and (15) are the open loop transfer functions from i_g to i^*_g when the L_f- C_f voltage and current are sensed respectively, which can be expressed as:

$$\frac{i_g(z)}{i^*_g(z)} = G_c(z) \cdot \frac{G_{u_i \to u_{LC}}(z)}{z + K(z)G_{u_i \to u_{LC}}(z)} \cdot \frac{i_g(z)}{u_{LC}(z)} \tag{14}$$

$$\frac{i_g(z)}{i^*_g(z)} = G_c(z) \cdot \frac{G_{u_i \to i_c}(z)}{z + K(z)G_{u_i \to i_c}(z)} \cdot \frac{i_g(z)}{i_c(z)} \tag{15}$$

The discrete PR controller at the fundamental frequency ω_o is listed with forward or Backward Euler discretization [24]. The discrete PR is given by:

$$G_c(z) = K_p + K_{i1} \frac{-T_s z^{-2} + T_s z^{-1}}{z^{-2} + (T_s^2 \omega_0^2 - 2)z^{-1} + 1} \quad (16)$$

G_c (z) can be reduced to K_p since the resonance gain has negligible effect above the fundamental frequency ω_o.

B. Design and Analysis of the Active damping based on Root-Locus

Then Root Loci analysis studying the of variation in active damping gain k for different methods with a given K_p are shown in Fig. 12. The gain K_p of the controlor $G_c(z)$ is set at the critical stable state without active damping and the value of K_p is 23.9. Then different active damping methods can be analyzed. Capacitor current k feedback is similar to the L_f-C_f trap voltage ks feedback and the capacitor current k/s feedback is similar to L_f-C_f trap voltage k feedback. The differential term usually introduces high frequency noise and it is not used in practical application. So Fig. 12 only shows six active damping methods.

As shown in Fig. 12, the solid line shows the root loci when k is larger than 0 (feedback) and the dotted line shows the root loci when k is smaller than 0 (feedforward). It can be seen in Fig. 12(a), when L_f-C_f trap voltage is controlled with proportional k active damping the system can be stable when k is negative and it is in fact a feedforward method. The stable period of k is from 0 to 0.3. At the critical stable state the system cannot be stable, when k is positive.

As shown in Fig. 12(b) when L_f-C_f trap voltage is controlled with k/s active damping, the system can be stable when feedforward control is used. The stable period of k is from 0 to 15200. When L_f-C_f trap voltage is controlled with $k/(s+\tau)$, as shown in Fig. 12(c), k should also be negative and the poles trend to move inside the unit circle again with τ increasing.

As shown in Fig. 12(d), when the capacitor current is controlled with k feedback the system can be stable when k is positive. When k increases to 11.6, the system becomes unstable again. When the capacitor current is controlled with $ks/(s+\tau)$ feedback the system can be stable when k is positive. With increasing τ of the high pass filter, the stable region of the system is larger. The maximum k can be obtained according to the root loci with different τ. When the capacitor current is controlled with $k/(s+\tau)$ (low-pass) feedback the system can be stable if k is positive, but the stable region is very small which matches the analysis using the equivalent impedance method before.

C. Comparision of Different Active Damping Methods

According to the virtual impedance-based analysis and designed parameters of different active damping methods, the comparisons are shown in Table IV. When L_f-C_f trap voltage u_{LC} with proportional and low pass control are used, the feedforward method should be applied to make the system stable. When the capacitor current i_c with proportional, low pass and high pass control are used, the feedback method
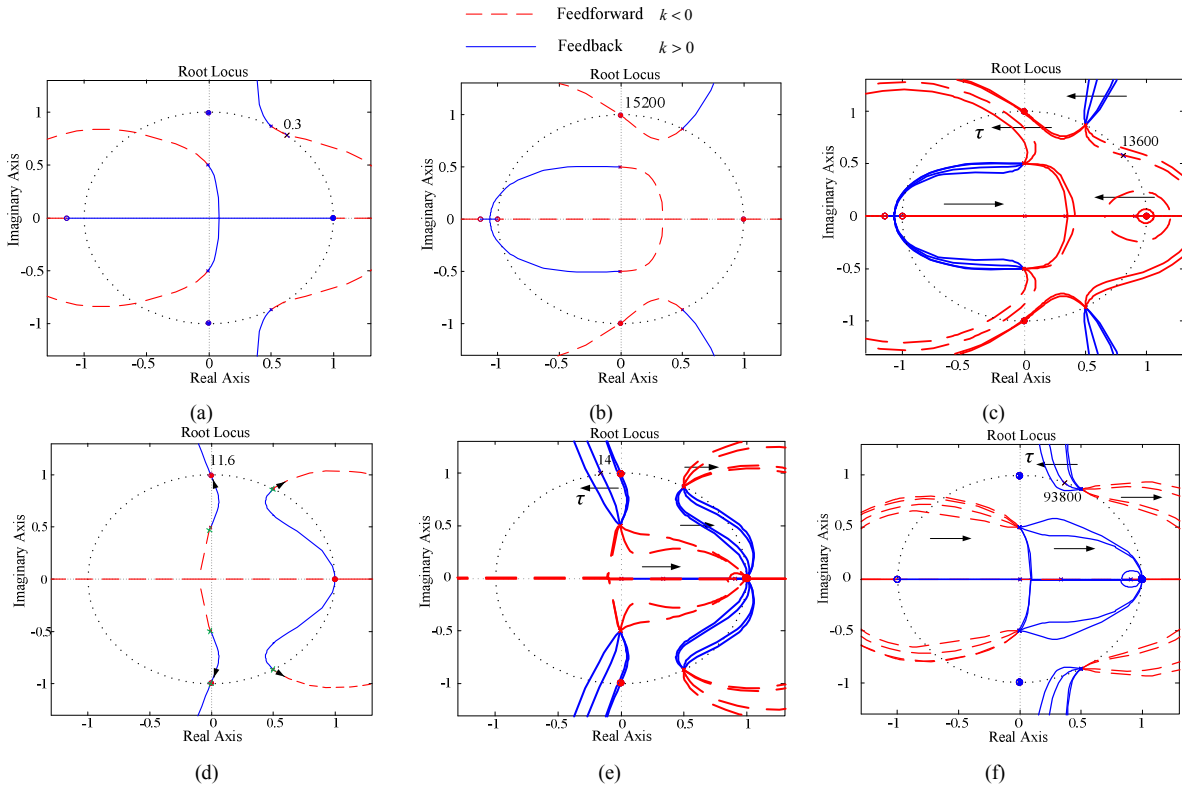

Fig. 12. Root loci of the variation in active damping gain k for a given K_p using L_f-C_f trap voltage feedback using the parameters in Table I. (a) k (b) k/s (c) $k/(s+\tau)$ and capacitor current feedback (d) k (e) $ks/(s+\tau)$ (f) $k/(s+\tau)$.

TABLE IV   Comparison of Different Active Damping Methods

Active damping	u_{LC} control		i_c control		
Feedback coefficient	k	$k/(s+\tau)$ (Low pass)	k	$ks/(s+\tau)$ (high pass)	$k/(s+\tau)$(Low pass)
Stability	feedforward	feedforward	feedback	feedback	feedback
Critical frequency f_n	$f_s/3$	$f_s/3$	$f_s/6$	$f_s/6 - f_s/3$	$0 - f_s/6$
Robustness	++	++	0	+	0

(a)   (b)   (c)
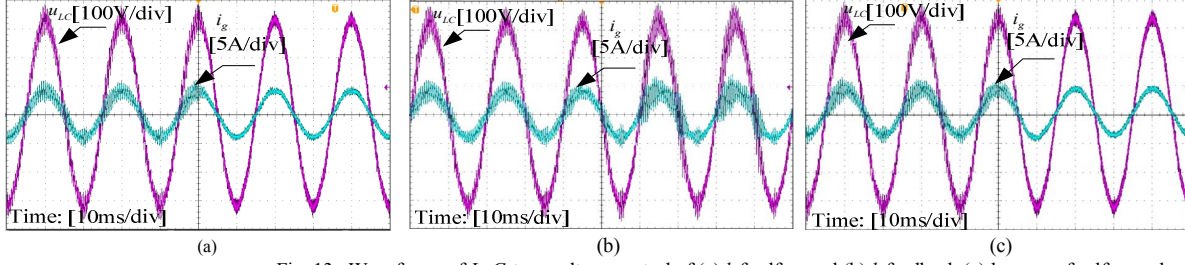
Fig. 13. Waveforms of L_f-C_f trap voltage control of (a) k feedforward (b) k feedback (c) low pass feedforward.

(a)   (b)   (c)
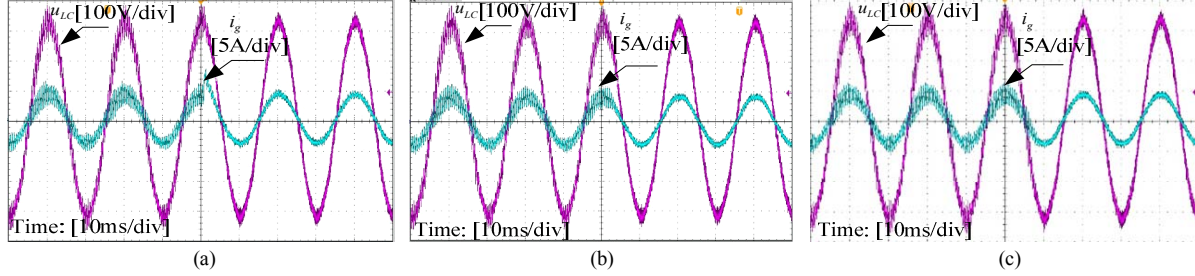
Fig. 14. Waveforms of capacitor current control of (a) k feedback (b) high pass feedback (c) low pass feedback are enabled.

(a)   (b)   (c)
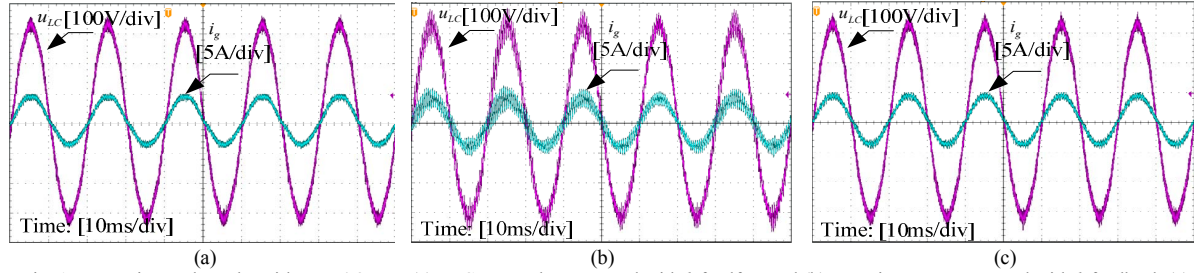
Fig. 15. Experimental results with L_g = 4.8 mH. (a) L_f-C_f trap voltage control with k feedforward (b) capacitor current control with k feedback (c) capacitor current control with high pass feedback.

should be applied to make the system stable. In terms of the robustness against the grid-impedance variation of different active damping methods, L_f-C_f trap voltage u_{LC} with proportional, low pass control and capacitor current i_c with high pass control are better to select.

V.   EXPERIMENTAL RESULTS

The experimental setup consists of a 2.2 kW Danfoss FC302 converter connected to the grid through an isolating transformer and the DC-link is supplied by Delta Elektronika power sources. The control algorithm has been implemented in a dSPACE DS1103 real time system. The aim of this section is to test the current control for the stability analysis with the different types of active damping control. The system parameters are given in TABLE I.

The controller gain is set to be 23.9 to make the system initially unstable and active damping methods are activated in the middle. Fig. 13(a) shows the waveforms when L_f-C_f trap circuit voltage proportional feed forward is used and k is

designed to 0.25 and the system becomes stable. When k is set to positive as feedback of the system is still unstable as shown in Fig. 13(b). It means for L_f-C_f trap circuit voltage proportional active damping method, feedforward has the damping effect and feedback does not have. This is in good agreement with the theoretical analysis. Fig. 13(c) shows the experimental waveforms when low pass feedforward is used. The k is set as 12200 and τ is set as 10000.

Fig. 14 shows the experimental results when the capacitor current control with k feedback is used, a high pass feedback and a low pass feedback are enabled. The system turns to be stable after these active damping methods are enabled.

Fig. 15 shows the experimental results with L_g = 4.8 mH for different active damping methods. It can be seen from Fig.15, for capacitor current active damping with k feedback, the current control is not stable. But for capacitor current active damping with high pass feedback and L_f-C_f trap voltage control with k feedforward, the current control is stable.

VI. Conclusions

This paper analyses the stability of the grid-connected inverter with *LLCL*-filter using different active damping methods based on the virtual impedance. The principle of virtual impedance method of the L_f-C_f circuit voltage and capacitor current with and without delay effect is presented by the equivalent impedance functions and circuits.

(1) L_f -C_f trap circuit of *LLCL*-filter perform capacitance characteristic before the switching frequency, so the extra L_f in the equivalent impedance does not influence the control of active damping and it is similar to the *LCL*-filter.

(2) The virtual impedance models show the essential principle of different active damping methods.

(3) It can be seen that different feedback coefficients can be used as active damping methods to suppress the resonance with a suitable design. L_f -C_f trap voltage with k and $k/(s+\tau)$ active damping should use a feedforward method. L_f -C_f trap voltage with $k/(s+\tau)$, capacitor current with k, $ks/(s+\tau)$ and $ks/(s+\tau)$ should use the feedback method.

(4) For L_f -C_f trap voltage with k feedforward the critical frequency f_n is one-third of the sampling frequency and for the capacitor current with k feedback the critical frequency f_n is one-sixth of the sampling frequency. Hence, L_f -C_f trap voltage feedback with k feedforward method has a better robustness for the variation of the resonant frequency due to the grid impedance variation. And for L_f -C_f trap voltage with $k/(s+\tau)$ feedforward method and capacitor current with $ks/(s+\tau)$ feedback method, the open-loop unstable Right Half-Plane poles caused by negative resistance can also be moved behind one-sixth of the sampling frequency with a suitable design of τ.

(5) Root loci are used to analyze the stability and design of these active damping methods in the z-domain. The experimental results match the active damping design and analysis well.

References

[1] F. Blaabjerg, R. Teodorescu, M. Liserre, and A. Timbus, "Overview of control and grid synchronization for distributed power generation systems," *IEEE Trans. Ind. Electron.*, vol. 53, no. 5, pp. 1398–1409, Oct. 2006.

[2] Y. Liu, C. Farnell, H. Zhang, A. Escobar, H. A. Mantooth, J. C. Balda, " A Silicon Carbide Fault Current Limiter for Distribution Systems," in Proc. Energy Conversion Congress and Exposition (ECCE), Sep 2014.

[3] M. Liserre, F. Blaabjerg, and S. Hansen, "Design and control of an *LCL*-filter-based three-phase active rectifiers," *IEEE Trans. Ind. Appl.*, vol. 41, no. 5, pp. 1281-1291, Sept./Oct. 2005.

[4] M. Liserre, R. Teodorescu, and F. Blaabjerg, "Stability of Photovoltaic and Wind Turbine Grid-Connected Inverters for a Large Set of Grid Impedance Values," *IEEE Trans. Power Electron.*, vol. 21, no. 1, pp. 263–272, Jan. 2006.

[5] W. Wu, Y. He, and F. Blaabjerg, "An LLCL power filter for single-phase grid-tied inverter," *IEEE Trans. Power Electron.*, vol. 27, no. 2, pp. 782-789, Feb. 2012.

[6] M. Huang, W. Wu, Y. Yang, and F. Blaabjerg, "Step by Step Design of a High Order Power Filter for Three-Phase Three-Wire Grid-connected Inverter in Renewable Energy System" in *Proc. PEDG* 2013, pp.1-8.

[7] A.M. Cantarellas, E. Rakhshani, D. Remon, and P. Rodriguez, "Design of the LCL+Trap Filter for the Two-Level VSC Installed in a Large-Scale Wave Power Plant," in *Proc. ECCE* 2013, pp. 707-712.

[8] J. M. Bloemink, and T C. Green, "Reducing Passive Filter Sizes with Tuned Traps for Distribution Level Power Electronics," in *Proc. IEEE EPE* 2011, pp. 1-9, Aug. 2011.

[9] C. Bao, X. Ruan, X. Wang, W. Li, D. Pan, and K, Weng, "Step-by-Step Controller Design for LCL-Type Grid-Connected Inverter with Capacitor–Current-Feedback Active-Damping," *IEEE Trans. Power Electron.*, vol. 29, no. 3, pp. 1239–1253, 2014.

[10] D. Pan, X. Ruan, C. bao, W. Li, and X. Wang, "Capacitor-Current-Feedback Active Damping With Reduced Computation Delay for Improving Robustness of LCL-Type Grid-Connected Inverter," *IEEE Trans. Power Electron.*, vol. 29, no. 7, pp.3414-3427, 2014.

[11] S. Parker, B. McGrath , and D.G. Holmes. "Regions of Active Damping Control for LCL Filters," *IEEE Trans. Ind. App.*, vol. 50, no. 1, pp.424-432, 2014.

[12] X. Wang, F. Blaabjerg, and P. C. Loh, "Virtual RC damping of LCL-filtered voltage source converters with extended selective harmonic compensation, " *IEEE Trans. Power Electron.*, early access, 2014.

[13] X. Wang, F. Blaabjerg, and P. C. Loh, "Analysis and design of grid-current-feedback active damping for LCL resonance in grid-connected voltage source converters, " in *Proc. IEEE ECCE* 2014, pp. 373-380.

[14] J. Dannehl, F. W. Fuchs, and S. Hansen, "Investigation of active damping approaches for PI-based current control of grid-connected pulse width modulation converters with LCL filters," *IEEE Trans. Ind. App.* , vol. 46, no. 4, pp.1509-1517, 2010.

[15] R. Peña-Alzola, M. Liserre, F. Blaabjerg, R. Sebastián, J. Dannehl, and F.W. Fuchs, "Analysis of the Passive Damping Losses in LCL-Filter-Based Grid Converters," *IEEE Trans. Power Electron.*, vol. 28, no. 6, pp. 2642-2646, June 2013.

[16] P. Channegowda and V. John, "Filter Optimization for Grid Interactive Voltage Source Inverters", *IEEE Trans. on Ind. Electron.*, vol. 57, no. 12, pp. 4106–4114, Dec. 2010.

[17] W. Wu, Y. He, and F. Blaabjerg, "A New Design Method for the Passive Damped LCL- and LLCL-Filter Based Single-Phase Grid-tied Inverter," *IEEE Trans. Ind. Electron.*, vol. 60, no. 10, pp. 4339-4350, Oct. 2013.

[18] W. Wu, M. Huang, Y. Sun, X. Wang, and F. Blaabjerg, "A composite passive damping method of the LLCL-filter based grid-tied inverter," In *Proc. of PEDG* 2012, pp.759 – 766, June 2012.

[19] M. Huang, P. C. Loh, W. Wu and F. Blaabjerg, "Stability Analysis and Active Damping for LLCL-filter Based Grid-Connected Inverters," in *Proc. IPEC* 2014, pp. 2610-2617.

[20] C. Zou, B. Liu, S. Duan, and R. Li, "Influence of Delay on System Stability and Delay Optimization of Grid-Connected Inverters with LCL Filter," *IEEE Trans. Ind. Info.*, vol. 10, no. 3, pp. 1775 - 1784, 2014.

[21] D. G. Holmes, T. A. Lipo, B. P. McGrath and W. Y. Kong, "Optimized design of stationary frame three phase AC current regulators, " *IEEE Trans. Power Electron.*, vol. 24, no. 11, pp. 2417-2425, Nov. 2009.

[22] J. Dannehl, M. Liserre, and F. W. Fuchs, "Filter-Based Active Damping of Voltage Source Converters With LCL Filter," *IEEE Trans. Ind. Electron.,*, vol. 58, no. 8, pp. 3623-3633, 2011.

[23] M. Orellana and R. Griñó, "On the stability of discrete-time active damping methods for VSI converters with a LCL input filter," in *Proc. IEEE IECON*, pp. 2378−2383, 2012.

[24] A.G. Yepes, F.D. Freijedo, J. Doval-Gandoy, O. López, J. Malvar, and P. Fernandez-Comesaña, "Effects of Discretization Methods on the Performance of Resonant Controllers," *IEEE Trans. Power Electron.*, vol. 25, no. 7, pp. 1692–1712, Oct. 2010.